IRAQI JOURNAL OF APPLIED PHYSICS LETTERS

The Iraqi Journal of Applied Physics Letters (IJAPLett) is a peer reviewed journal of high quality devoted to the publication of original research letters from applied physics and their broad range of applications. IJAPLett publishes quality original research letters in physics and its applications in the broadest sense. It is intended that the journal may act as an interdisciplinary forum for physics and its applications. Innovative applications and material that brings together diverse areas of physics are particularly welcome. IJAPLett aims to disseminate knowledge; provide a learned reference in the field; and establish channels of communication between academic and research experts, policy makers and executives in industry, commerce and investment institutions. IJAPLett is a quarterly specialized periodical dedicated to publishing original letters in: Alternative & Renewable Energy, Applied Mechanics & Thermodynamics, Applied Optics & Optical Design, Biophysics & Bioengineering, Cryptography & Applications, Electromagnetic Fields, Electronic Materials & Devices, Energy Generation & Conversion, Fluids Physics & Mechanics, Imaging, Microscopy & Spectroscopy, Laser Physics & Applications, Magnetism & Applications, Instrumentation, Measurements & Metrology, Nanostructures & Applications, Nonlinear & Ultrafast Optics, Nuclear Physics & Engineering, Optical Communications & Systems, Optoelectronics Devices & Applications, Organic Materials, Devices & Applications, Physical Chemistry & Biochemistry, Plasma, Discharge Physics & Applications, Quantum Physics & Spectroscopy, RF & Digital Communications, Semiconductors & Devices, Simulation & Modeling Research, Solar Energy & Devices, Solid State Physics & Applications, Structure & Properties of Matter, Superconductivity & Related Devices, Surfaces, Interfaces & Films, Thin Films & Applications, and Vacuum Science & Technology.

ISSN (Print)
1999-656X
ISSN (Online)
2958-6488

EDITORIAL BOARD

Editorial Office:
P. O. Box 88052, Baghdad 12631, IRAQ
Website: www.iraqiphysicsjournal.com
Emails: editor@iraqiphysicsjournal.com, editor_ijap@yahoo.co.uk, ijaplett.editor@gmail.com

ADVISORY BOARD

SPONSORED AND PUBLISHED BY
AMERICAN QUALITY FOR SCIENTIFIC PUBLISHING INC.
1479 South De Gaulle Ct, Aurora, CO 80018, United States

IRAQI JOURNAL OF APPLIED PHYSICS LETTERS

ISSN (Print): 1999-656X, ISSN (Online): 2958-6488

INSTRUCTIONS TO AUTHORS

CONTRIBUTIONS

Contributions to be published in this journal should be original research works, i.e., those not already published or submitted for publication elsewhere, individual papers or letters to editor.
Manuscripts should be submitted to the editor at the mailing address:

Iraqi Journal of Applied Physics Letters, Editorial Board, P. O. Box 88052, Baghdad 12631, IRAQ
Website: www.iraqiphysicsjournal.com
Email: editor@iraqiphysicsjournal.com, editor_ijap@yahoo.co.uk, ijaplett.editor@gmail.com

MANUSCRIPTS

Two hard copies with soft Word copy on a CD or DVD should be submitted to Editor in the following configuration:

- **One-column** Double-spaced one-side A4 size with 2.5 cm margins of all sides
- Times New Roman font (16pt bold for title, 14pt bold for names, 12pt bold for headings, 12pt regular for text)
- Manuscripts presented in English only are accepted.
- English abstract not exceed 100 words
- 4 keywords (at least) should be maintained on (PACS preferred)
- Author(s) should express all quantities in SI units
- Equations should be written in equation form (*italic* and symbolic) NOT in plain text
- Tables and Figures should be separated from text and placed in new pages after the references
- Charts should be indicated by the software used for generating them (e.g., Excel, MATLAB, Grapher, etc.)
- Figures and diagrams can be submitted in original colored forms for assessment and they will be returned to authors after provide printable copies
- Only original or high-resolution scanner photos are accepted
- For electronic submission, articles should be formatted with MS-Word software.

AUTHOR NAMES AND AFFILIATIONS

It is IJAPLett policy that all those who have participated significantly in the technical aspects of a paper be recognized as co-authors or cited in the acknowledgments. In the case of a paper with more than one author, correspondence concerning the paper will be sent to the first author unless staff is advised otherwise.
Author name should consist of first name, middle initial, last name. The author affiliation should consist of the following, as applicable, in the order noted:
- Company or college (with department name or company division), Postal address, City, Governorate or State, zip code, Country name, contacting telephone number, and e-mail

REFERENCES

The references should be brought at the end of the article, and numbered in the order of their appearance in the paper. The reference list should be cited in accordance with the following examples:
[1] X. Ning, R. Benford and M.R. Lovell, "On the Sliding Friction Characteristics of Unidirectional Continuous FRP Composites", *J. Tribol. Func. Mater.*, 124(1) (2002) 5-13.
[2] M. Barnes, "Stresses in Solenoids", *J. Appl. Phys.*, 48(5) (2001) 2000–2008.
[3] J. Jones, **"Contact Mechanics"**, Cambridge University Press (Cambridge, UK) (2000), Ch.6, p.56.
[4] Y. Lee, S.A. Korpela and R. Horne, "Structure of Multi-Cellular Natural Convection in a Tall Vertical Annulus", Proceedings of 7th International Heat Transfer Conference, U. Grigul et al., eds., Hemisphere (Washington DC), 2 (1982) 221–226.
[5] M. Hashish, "Waterjet Technology Development", High Pressure Technology, PVP-Vol. 406 (2000) 135-140.
[6] D.W. Watson, "Thermodynamic Analysis", ASME Paper No. 97-GT-288 (1997).
[7] C.Y. Tung, "Evaporative Heat Transfer in the Contact Line of a Mixture", Ph.D. thesis, Rensselaer Polytechnic Institute, Troy, NY (1982).

PROOFS

Authors will receive proofs of papers and are requested to return one corrected copy as a WORD file on a compact disc (CD) or by email. New materials inserted in the original text without Editor's permission may cause rejection of paper unless the handling editor is informed.

COPYRIGHT FORM

Author(s) will be asked to sign the IJAPLett Copyright Form and hence transfer copyrights of the article to the Journal soon after acceptance of it. This will ensure the widest possible dissemination of information.

OFFPRINTS

Authors will receive electronic offprint free of charge and any additional reprints can be ordered.

SUBSCRIPTION AND ORDERS

Annual fees (4 issues per year) of subscription are:
50 US$ for individuals inside Iraq; **200** US$ for institutions inside Iraq;
100 US$ for individuals abroad; **300** US$ for institutions abroad.

Characterization of Tin Oxide Nanoparticles Prepared by Pulsed Laser Ablation and Their Use as Antibacterial Agents

Mays W. Skakir, Awatif S. Jasim

Department of Physics, College of Science, University of Tikrit, Tikrit, IRAQ

Abstract
In this work, preparation of tin nanoparticles using pulsed laser (Nd:YAG) ablation and the study of their physical properties and their antibacterial activity were presented. The results of biological tests confirmed that the prepared nanoparticles have good antibacterial activity. It was observed that the increase in the number of laser pulses led to an increase in the antibacterial activity of all the prepared nanoparticles.

Keywords: Tin dioxide; Nanoparticles; Structural phase; Reactive sputtering; Solvothermal method
Received: 17 May 2023; **Revised:** 11 June 2023; **Accepted:** 18 June 2023; **Published:** 1 September 2023

1. Introduction

The fields of science and industry have recently embraced nanotechnology as an emerging topic [1-6]. Nanoparticles have lately been utilized to circumvent this issue since they come into direct contact with bacterial cell walls without having to enter the cell, making them less likely to encourage bacterial resistance. Many metallic nanoparticles, such as zinc, titanium oxide, silver, gold, copper oxide, and tin, have been created for use as antibacterial agents [7-12]. Recent years have seen a rise in the production of tin oxide nanoparticles for a variety of uses, including antibacterial agents [13-15]. The physical process of pulse laser ablation in a liquid medium is the alternative methodology [16]. An energy source such as a pulsed Nd:YAG laser is frequently employed in this technique to ablate materials and generate a bright plasma [17-18]. Following the condensing of the plasma in the liquid medium, the liquid medium is subsequently filled with nanoparticles. Using a pulse laser ablation technique, we created tin oxide nanoparticles and studied their physical properties [19-20]. Tin oxide nanoparticles were prepared using a liquid medium of ethanol with varied solution concentrations. Therefore, SnO_2 NPs were then applied as an antibacterial agent against positive bacteria (*Streptococcus mutans*) and negative bacteria (*Escherichia coli*) as well as *Candida albicans* that were isolated from the oral cavity to test the properties of the nanoparticles produced and determine their antibacterial activity, as it was shown that the higher the concentration of tin oxide nanoparticles, the greater the ability to degrade bacteria and discourage them.

2. Experimental Part

A Q-switched Nd:YAG laser with wavelength of 1064 nm and energy of 100 mJ was used to synthesize SnO_2 NPs in 3 mL highly-pure ethanol (99.99%), which was placed 15 cm away from the laser source. The repetition rate of laser irradiation was 5 Hz at different number of pulses (50, 100, 150, 200, and 250). As a result, the brownish-yellow colloidal nanoparticles are successfully formed in all samples shortly after laser irradiation on the high-purity tin metal plate. The color of those colloids is almost identical to the brownish colloidal tin nanoparticles prepared in various liquid media [21-22].

The morphological characteristics of the prepared nanoparticles were determined

using the transmission electron microscopy (TEM).

Positive bacteria (*Streptococcus mutans*) and negative bacteria (*Escherichia coli*) as well as *Candida albicans* that were isolated from the oral cavity were used to test the properties of the produced nanoparticles and to determine their antibacterial activity. The diameter of the inhibition zone (DIZ), a sign of an inhibitory reaction to the inhibition of bacterial growth by the antibacterial component in the extract, was measured using the disc diffusion technique. The inhibitory zone diameter was measured after the test media had been incubated at 37°C for 18 to 24 hours.

3. Results and Discussion

The TEM images of the colloidal tin oxide nanoparticles are shown in figures (1) and (2). The prepared nanoparticles have the same spherical shape, as can be seen [23]. When metal nanoparticles are synthesized using the pulsed laser ablation method, these spherical forms of nanoparticles are frequently formed. Tin oxide nanoparticles can easily be formed from tin nanoparticles produced by pulsed laser ablation in a liquid medium [24].

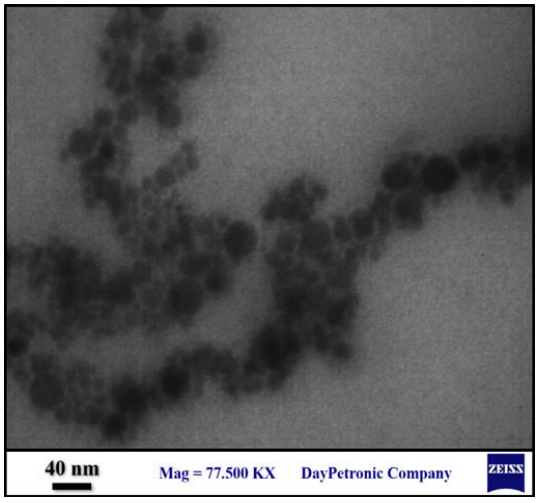

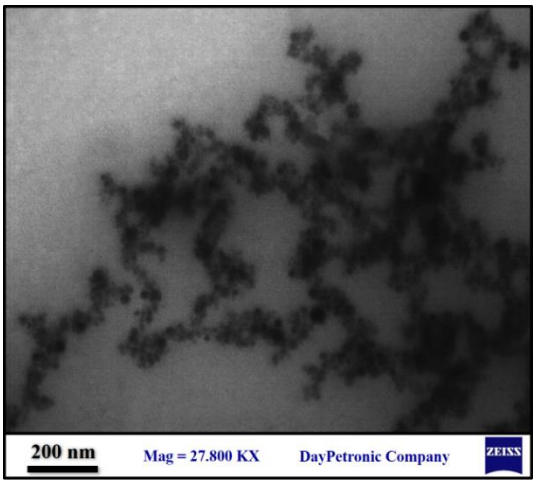

Fig. (5) TEM images of a solution of SnO_2 NPs particles at different scales (40 and 200 nm) in low concentration

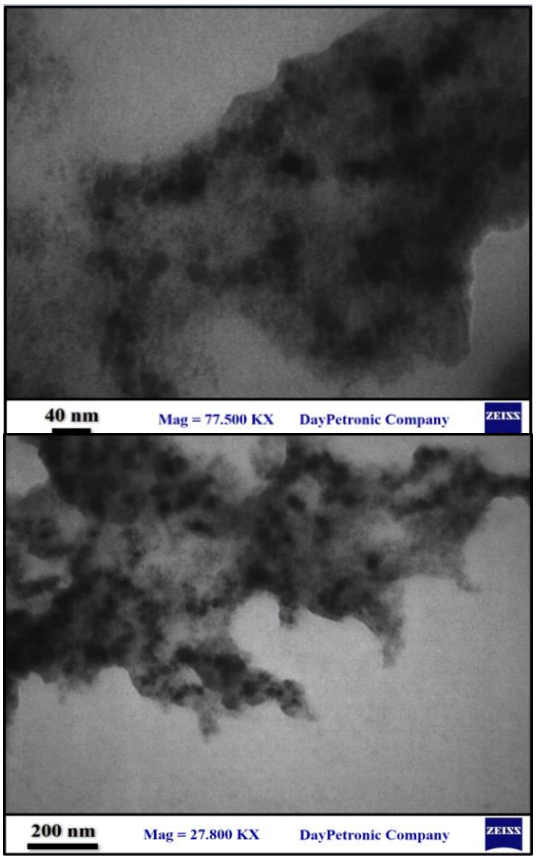

Fig. (6) TEM images of a solution of SnO_2 NPs particles at different scales (40 and 200 nm) in high concentration

The prepared tin oxide nanoparticles were subsequently tested at different concentrations, as shown in figure (3) and (4). As the concentration of tin oxide nanoparticles increases, the diameter of the inhibition zone expands, increasing the amount of bacterial activity inhibited. Similar pattern was also recently reported

[25]. This state is explained by the fact that as the concentration of SnO_2 nanoparticles increases, more of the tiny particles are taken up by bacterial cells, increasing the rate at which they dehydrate.

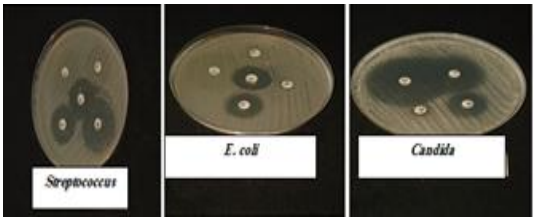

Fig. (7) Antibiotic sensitivity test of E. coli, Streptococcus, and Candida respectively

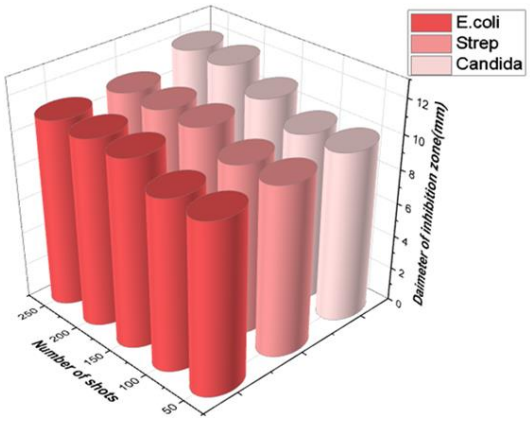

Fig. (8) Histogram of SnO_2 NPs antibacterial activity according to the diameters of inhibition zones when prepared at the wavelength 1064nm

The respiration mechanism that takes place in the bacterial cell membrane causes dehydrogenation to happen. After interacting with the nanoparticles, the bacteria start to deactivate their enzymes, which results in the production of hydrogen peroxide, which kills the bacteria [26]. This outcome proved that the tin oxide nanoparticles created in this work can be used as an antibacterial agent for both gram-negative and gram-positive microorganisms, like strep and E. coli, respectively.

4. Conclusions

Measurements of antibacterial activity of tin oxide nanoparticles prepared by pulsed laser ablation revealed that they can be used against Gram positive and negative bacterial as well as fungi. The highest DIZ value for the highest concentration demonstrates how the higher concentrations of tin oxide nanoparticles enhance the inhibition zone of bacterial activity for both types of bacteria.

References

[1] S. Rai and A. Rai, "Nanotechnology: The secret of fifth industrial revolution and the future of next generation", J. Nasional, 7(2) (2017) 61-66.

[2] A. Khumaeni et al., "Characteristics of tin oxide nanoparticles produced by pulsed laser ablation technique in various concentrations of chitosan liquid and their potential application as an antibacterial agent", Resul. Eng., 16 (2022) 100742.

[3] S.M. Solaiman et al., "Nanotechnology and its medical applications: revisiting public policies from a regulatory perspective in Australia", Nanotechnol. Rev., 6(3) (2017) 255-269.

[4] X. He and H.M. Hwang, "Nanotechnology in food science: Functionality, applicability, and safety assessment", J. Food Drug Anal., 24(4) (2016) 671-681.

[5] W. Hannah and P.B. Thompson, "Nanotechnology, risk and the environment: a review", J. Enviro. Monitor., 10(3) (2008) 291-300.

[6] B.G. Priestly, A.J. Harford and M.R. Sim, "Nanotechnology: a promising new technology - but how safe?" Med. J. Australia, 186(4) (2007) 187-188.

[7] Y. Xie et al., "Antibacterial activity and mechanism of action of zinc oxide nanoparticles against *Campylobacter jejuni*", Appl. Enviro. Microbiol., 77(7) (2011) 2325-2331.

[8] M. Azizi-Lalabadi et al., "Antimicrobial activity of Titanium dioxide and Zinc oxide nanoparticles supported in 4A zeolite and evaluation the morphological characteristic", Sci. Rep., 9(1) (2019) 17439.

[9] G. Franci et al., "Silver nanoparticles as potential antibacterial agents", Molecules, 20(5) (2015) 8856-8874.

[10] X. Li et al., "Functional gold nanoparticles as potent antimicrobial agents against multi-drug-resistant bacteria", ACS Nano, 8(10) (2014) 10682-10686.

[11] D. Sistemática et al., "Copper nanoparticles as potential antimicrobial agent in disinfecting root canals. A systematic review", Int. J. Odontost., 10(3) (2016) 547-554.

[12] S.M. Amininezhad et al., "The antibacterial activity of SnO_2 nanoparticles against Escherichia coli and Staphylococcus aureus", Zahedan J. Res. Med. Sci., 17(9) (2015).

[13] Y.T. Gebreslassie and H.G. Gebretnsae, "Green and cost-effective synthesis of tin oxide nanoparticles: a review on the synthesis methodologies, mechanism of formation, and

their potential applications", Nanoscale Res. Lett., 16(1) (2021) 97.
[14] V.K. Vidhu and D. Philip, "Biogenic synthesis of SnO2 nanoparticles: evaluation of antibacterial and antioxidant activities", Spectrochim. Acta Part A: Mol. Biomol. Spectro., 134 (2015) 372-379.
[15] D.C. Sekhar, B.S. Diwakar and N. Madhavi, "Synthesis, characterization and anti-bacterial screening of complex nanocomposite structures of SiO_2@ZnO@Fe_3O_4 and SnO_2@ZnO@ Fe_3O_4", Nano-Struct. Nano-Objects, 19 (2019) 100374.
[16] M. Dell'Aglio et al., "Mechanisms and processes of pulsed laser ablation in liquids during nanoparticle production", Appl. Surf. Sci., 348 (2015) 4-9.
[17] T.A. Labutin et al., "Femtosecond laser-induced breakdown spectroscopy", J. Anal. Atom. Spectro., 31(1) (2016) 90-118.
[18] A. Khumaeni et al., "Characteristics of tin oxide nanoparticles produced by pulsed laser ablation technique in various concentrations of chitosan liquid and their potential application as an antibacterial agent", Res. Eng., 16 (2022) 100742.
[19] M.A. Gondal, Q.A. Drmosh and T.A. Saleh, "Preparation and characterization of SnO_2 nanoparticles using high power pulsed laser", Appl. Surf. Sci., 256(23) (2010) 7067-7070.
[20] A. Qona'ah, I. Nurhasanah and A. Khumaeni, "Synthesis of tin oxide nanoparticles by pulsed laser ablation method using low-energy Nd:YAG laser as an antibacterial agent", J. Nano Res., 68 (2021) 114-122.
[21] D.K. Naser, A.K. Abbas and K.A. Aadim, "Zeta potential of Ag, Cu, ZnO, CdO and Sn nanoparticles prepared by pulse laser ablation in liquid environment", Iraqi J. Sci., (2020) 2570-2581.
[22] R.A. Ismail et al., "Pulsed laser ablation of tin oxide nanoparticles in liquid for optoelectronic devices", Silicon, 13 (2021) 3229-3237.
[23] F. Mafuñe et al., J. Phys. Chem. B, 104 (2000) 39, https://doi.org/10.1021/jp001803b.
[24] M. Li, Q. Lu and Z. Wang, "Preparation of tin oxide nanoparticles by laser ablation in solution", Int. J. Nanosci., 5(2-3) (2006) 259-264.
[25] A. Khumaeni et al., "Characteristics of tin oxide nanoparticles produced by pulsed laser ablation technique in various concentrations of chitosan liquid and their potential application as an antibacterial agent", Res. Eng., 16 (2022) 100742.
[26] P. Kamaraj et al., "Biological activities of tin oxide nanoparticles synthesized using plant extract", World J. Pharm. Pharm. Sci., 3(9) (2014) 382-388.

Cavity-Ring Down Absorption of Ammonia to Tunable Extended-Cavity Diode Laser Radiation

Oday A. Hammadi

Department of Physics, College of Education, Al-Iraqia University, Baghdad, Iraq

Abstract

The CRD technique has been successfully applied in various environments since it directly provides the frequency-dependent absorption strengths of the medium under study. As mirrors with a sufficiently high reflectivity, detectors with a sufficiently fast time response, and tunable (pulsed) light sources are available, there is no intrinsic limitation to the spectral region in which CRD can be applied. In this work, cavity-ring down (CRD) technique was employed to stabilize the absorption of a cell filled with ammonia gas to 120μs pulses from a 904nm GaAlAsP semiconductor laser.

Keywords: Cavity-ring down technique; Ammonia absorption; Laser diagnostics; Laser applications
Received: 17 May 2023; **Revised:** 11 June 2023; **Accepted:** 18 June 2023; **Published:** 1 September 2023

1. Introduction

When a fast laser pulse is transmitted into the ring-down cavity, it will gradually leak out of the cavity as a small fraction of the light is transmitted through the mirrors at each reflection [1]. If a detector is placed at the exit mirror, the signal recorded over time will behave where each pulse corresponds to one cavity round trip by the laser pulse [2]. Since CRDS measurements are independent of the initial source intensity, shot to shot fluctuations of the laser do not limit sensitivity [3]. In addition, the long absorption path-lengths (can be as high as a few km), which result from many laser round trips, further increase the sensitivity of this technique [4]. However, since the number of round trips, and therefore the path-length, is dependant upon the strength of the absorbing species, the sensitivity is generally reported as the minimum detectable fractional absorption per laser round trip [5].

If the light source is monochromatic (laser is an example), one can record an absorption spectrum of the sample by measuring the transmitted intensity as a function of the frequency. Alternatively, a broad light source can be used when the incident light or the transmitted light is spectrally dispersed [1].

To date, the cavity-ring down (CRD) technique has been successfully applied in various environments. High-resolution spectroscopy studies have been performed on molecules in cells and supersonic jets and on transient molecules generated in discharges, flow reactors and flames [6]. The CRD spectra directly provide the frequency-dependent absorption strengths of the molecules under study, which contain information on the number density, cross-section and temperature [7]. By now, successful application of CRD spectroscopy has been demonstrated from the ultraviolet (UV) part of the spectrum to the infrared (IR) spectral region [8].

In a typical CRD experiment, a light pulse with a spectral intensity distribution and a duration, which is shorter than the CRD time, is coupled into a non-confocal optical cavity consisting of two highly reflecting, mirrors [9]. The fraction of the light that is successfully coupled into the cavity bounces back and forth between the mirrors. The intensity of light inside the cavity decays as a function of time, since at each reflection of a mirror a small fraction of the light is coupled out of the cavity. Measuring the intensity of light exiting the cavity easily monitors time dependence of the intensity inside the cavity [10]. In an empty cavity,

this ring-down transient is a single-exponentially decaying function of time with a e^{-1} of CRD time which is solely determined by the reflectivity of the mirrors and the optical path length between the mirrors [10]. The presence of absorbing species in the cavity gives an additional loss channel for the light inside the cavity [11]. If the absorption follows Beer's law, the light intensity inside the cavity will still decay exponentially, resulting in a decrease in the CRD time [12].

In general, CRD is most applicable to making highly sensitive quantitative measurements of trace molecular gas phase species, performing time resolved kinetic studies on short lived or low concentration molecular species, and investigating weak molecular transitions from the UV up through the mid-IR spectral range [13,14].

When Beer's law behavior fails, CRDS can still be used to obtain quantitative information, but the reduction of this information to the absorption spectrum of the sample inside the cavity will require detailed knowledge about the pulse characteristics [15]. Consequently, we emphasize in this paper determining the conditions for which the ring-down waveform shows exponential decay as a function of time.

In this work, CRD technique has been successfully applied in various environments since it directly provides the frequency-dependent absorption strengths of the medium under study.

2. Experiment

There are no intrinsic limitations to the spectral region in which CRD can be applied, provided that mirrors with a sufficiently high reflectivity, detectors with a sufficiently fast time response, and tuneable-pulsed lasers are available. A typical experimental CRD set-up is given in Fig. (1). This basic set-up is fairly simple; it consists of LASERTRON pulsed tunable extended-cavity diode laser (ECDL) system including digital-controlled driving power supply (DCDPS), ring-down cavity, beam splitter (BS), focusing optics (L), 2 fast detectors (PD), 2 A/D converter, 2 signal amplifiers, 2 RS-232 interface cards, 7GHz spectrum analyzer (R&S FSE-B2), and PC for data handling and transformation. The testing elements include gas nozzles, comparison 4cm^3 ammonia-filled cell and rotary pump. The actual choice of these components depends on the wavelength region in which the CRD spectrum needs to be recorded.

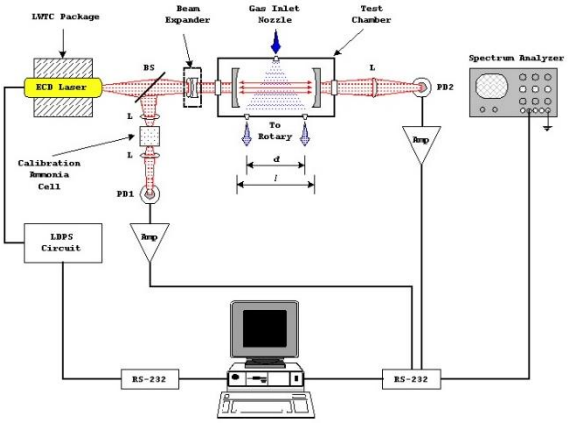

Fig. (1) The experimental set-up

Two identical concave mirrors form the ring-down cavity and the reflectivities and radii of curvature (r) are 0.99, 25cm and 0.95, 1m, respectively. The length (l) filled by gas in the CRD chamber is ~4cm and the mirrors are placed at a distance (d) and is adjustable from 1cm to 10cm that is $0<d<r$. The mirrors are placed on mounts to change their positions relative to each other in order to align the cavity. Experimentally, the distance d was varied from 4cm to 10cm since its minimum corresponds the distance (l) filled by ammonia.

The output laser wavelength is tuned over 894-914nm with <1nm resolution by changing laser cavity length (d). The maximum output power of laser diode used is ~5mW. Pulsating is achieved by the (DCDPS) with a pulse duration of ~120μs and pulse repetition rate (PPR) of 10Hz. After averaging the ring-down transients over a predefined number of laser pulses on the on-board memory of the spectrum analyzer, the data are transferred to the PC.

In the first attempts of experiment, a problem appeared that the laser beam directing to the test chamber is spread. Hence, beam expander optics were placed to keep laser beam guided. Flow rate of gas entering the test chamber is 10-50 liter/min as the maximum suction speed of the rotary pump is 50 liter/min.

3. Results and Discussion

The decay or CRD time (τ) was deduced to be few nanoseconds range. Fig. (2) shows the variation of absorption with the concentration of ammonia filling the test chamber. As shown, the absorption of gas to the laser wavelength increases as its concentration does. According to Beer-Lambert law, this increasing absorption saturates when the mean free path becomes small enough to admit more absorption. In this experiment, the concentrations of ammonia did not reach such level of saturation as confirmed by the continuous increasing of absorption.

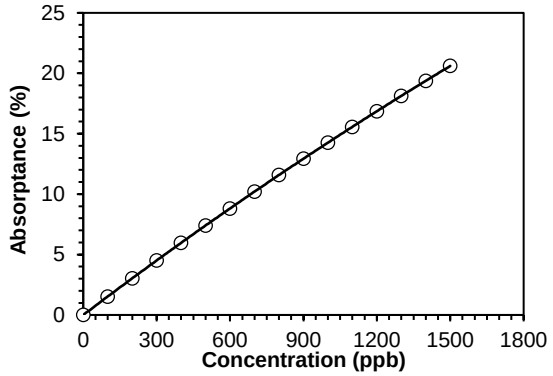

Fig. (2) Variation of absorptance (*A*) as a function of the NH_3 concentration inside the CRD chamber

As the spacing between the two mirrors of ring-down cavity is varied (4-10cm), the percent absorption was determined at the 0.909μm wavelength and the results are shown in Fig. (3). Though the distance filled by ammonia is practically constant (l~4cm), the absorption is increasing with the increasing distance (d). This is attributed to increasing volume of the effective medium (ring-down cavity) including the absorbing medium (NH_3). However, large distance caused laser beam to oscillate out of the cavity axis, which may be lost by diffraction at the edges of cavity.

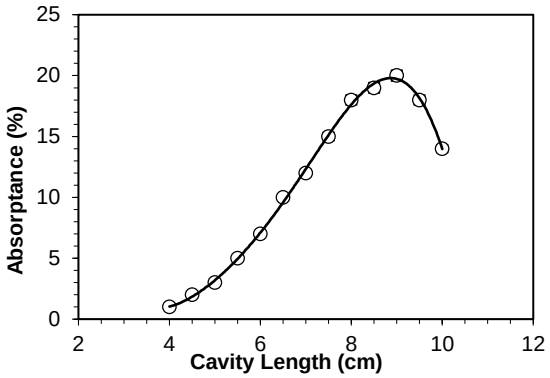

Fig. (3) Variation of absorptance of the NH_3-filled chamber with ring-down cavity length (spacing between CRD mirrors)

The deviation from exponential ring-down decay becomes significant for long observations times, which are associated with the pulse absorption pathlengths equal to several line-center absorption lengths. For the absorption pathlength shorter than, the decay remains approximately exponential, even if the pulse linewidth is wider than the absorption linewidth

Since the work aims to employ CRD technique in diagnostics, then the transmittance in Fig. (4) was measured as a function of input laser power at the optimum wavelength (0.909μm) and 1500ppb concentration. This measurement is required for calibration.

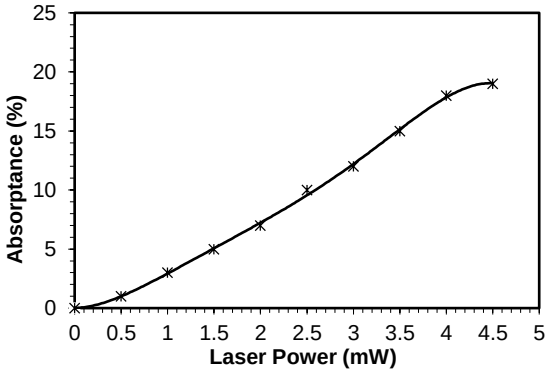

Fig. (4) Variation of absorptance (A) of the NH_3-filled chamber with laser power entering test chamber

The absorption of test chamber to the laser radiation was measured again with varying concentration of NH_3, as shown in Fig. (5). As soon as the detector receives the first transmitted signal, the readout is

converted into percent absorptance term and stored as a reference value. When the concentration is increased, the absorptance decreases, as in Fig. (2), hence, the second readout is compared to the first one. It is already lesser, so the control circuit increases driving current and hence output power. Accordingly, the transmitted, as well as the absorbed, part of radiation is increased to the reference level. As soon as the detector receives it, the former step is repeated. It should be noted that this procedure is performed while the laser wavelength remain constant (0.909μm). So, the interaction between laser radiation and gas medium can be described as "stable", as shown in Fig. (5).

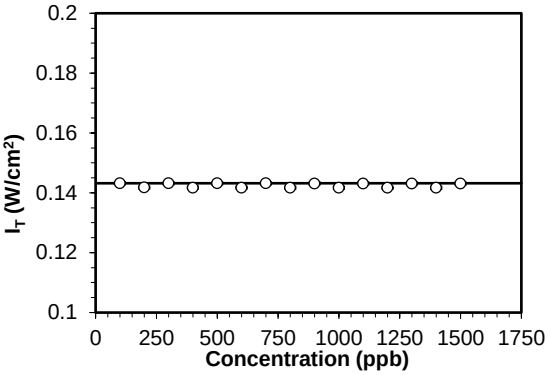

Fig. (5) Normalization of transmitted laser intensity (I_T) as a function of NH_3 concentration inside the CRD chamber

In practice, the length of the observation time is limited by the dynamic range of the detection system used to acquire and digitize the ring-down waveform. It is justified, therefore, to restrict the observation time to about 5τ, where τ is the ring-down time for the system [16]. During the observation time 5τ, the signal intensity decreases by about 99%. For sample absorption loss constituting about 10% of the total cavity loss, the observation time 5τ is associated with an absorbance value of 0.5.

4. Conclusions

In this work, cavity-ring down (CRD) technique was employed to introduce the absorption characteristics of a cell filled with ammonia gas to 120μs pulses from a 904nm GaAlAsP semiconductor laser. A stability of about 1% was achieved in the absorption response of a ring-down cavity to the laser radiation. This stability is obtained by optimizing the absorption parameters of gas medium filling the resonance cavity. Despite that such experiment has several parameters; it is simple, reliable, non-destructive and accurate (within ~1%) diagnostic technique in many applications such as trace gas detection, optical parametric oscillator (OPO), and fast absorption spectroscopy.

References

[1] R.T. Jongma, M. Boogaarts and I. Holleman, Rev. Sci. Instrum., 66 (1995) 2821.
[2] P. Zalicki and R.N. Zare, J. Chem. Phys., 102 (1995) 2708.
[3] R. Engeln, G. Berden and R. Peeters, Rev. Sci. Instrum., 69 (1998) 3763.
[4] G. Berden, R. Peeters and G. Meijer, Chem. Phys. Lett., 307 (199) 131.
[5] R. Peeters, G. Berden and A. Apituley, Appl. Phys. B, 71 (2000) 231.
[6] B.A. Paldus, C.C. Harb and T.G. Spence, Opt. Lett., 25 (2000) 666.
[7] J.D. Ayers, L. Apodaca and W.R. Simpson, Appl. Optics, 44 (2005) 7239.
[8] H.D. Osthoff, S.S. Brown and T.B. Reyrson, J. Geophys. Res., 111 (2006) D12305.
[9] H. Fuchs, W.P. Dube and S.G. Ciciora, Anal. Chem., 80 (2008) 6010.
[10] H. Fuchs, W.P. Dube and B.M. Lerner, Environ. Sci. Technol., 43 (2009) 7831.
[11] G. Schuster, I. Labazan and J.N. Crowley, Atmos. Meas. Tech., 2 (2009) 1.
[12] N.L. Wagner, W. Dube and R. Washefelder, Atmos. Meas. Tech., 4 (2011) 1227.
[13] S. James et al., J. Anal. Spectro., 18 (2018) 49-56.
[14] P. Woodward et al., J. Chem. Phys., 55 (2008) 101-110.
[15] C.J. Oxwald et al., Phys. Chem. Lett., 47 (2004) 215-220.
[16] P. Meystre and M. Sargent III, **"Elements of Quantum Optics"**, 2nd ed., Springer (Berlin, 1991).
[17] M. Dominquez et al., Proc. Quant. Opt., 13 (2010) 33-36.

Preparation and Characterization of Carbon Nitride Nanopowders by Glow Discharge-Induced Reaction

Sami M. Abdullah[1], Oday A. Hammadi[2], Laith R. Ghareeb[1]

[1] Department of Physics, College of Science, University of Sumer, Thi Qar, IRAQ
[2] Department of Physics, College of Education, Al-Iraqia University, Baghdad, IRAQ

Abstract
In this work, the reaction of methane and ammonia gases at room temperature was induced by electric power transferred to the reaction volume throughout argon fast glow discharge at high pressures. This power was applied to the reaction as short pulses to produce carbon nitride nanoparticles without production of cyanogen molecules. The growth and development of carbon nitride structures was confirmed by x-ray diffraction (XRD) and Fourier-transform infrared (FTIR) spectroscopy. The synthesized carbon nitride nanoparticles were polycrystalline and lower number of crystal planes was obtained using shorter pulses of discharge power.

Keywords: Carbon nitride; Nanoparticles; Glow discharge; Structural characteristics
Received: 22 August 2023; **Revised:** 16 September; **Accepted:** 24 September; **Published:** 1 October 2023

1. Introduction

Due to the increasing importance of carbon nitride nanostructures in various applications, intense research works were carried out during the last two decades on the synthesis as well as characterization of such structures. This compound is very interesting candidate for applications such nanocomposite with enhanced photocatalytic activity [1], nanocomposites [2], electrocatalyst [3], photochemical applications such as photoredox catalysis [4], metal-free catalysis [5-7], optoelectronics such as photodiodes [8] and tribology [9].

Carbon nitride has many formulas resulted from the bonding of carbon and nitrogen atoms, however, dicyanodiazomethane with the formula of C_3N_4 or $(CN)_2.C.N_2$ is one of the most important ones and has a 3D structure as shown in Fig. (1) [10,11]. It has two solid covalent network compounds: beta (β-C_3N_4) and graphitic (g-C_3N_4). The first is predicted to be harder than diamond while the second has very important catalytic properties [12-15].

Carbon nitride nanostructures are synthesized and prepared by various methods and techniques such as photoreduction [1], thermal evaporation [3], polymerization of some organic compounds [5,13], laser ablation in liquids [6], chemical vapor deposition [10], plasma decomposition of methane and molecular nitrogen [11], ball-milling at high temperatures [15], plasma-enhanced chemical vapor deposition [9,12,17], laser pyrolysis [18], RF reactive magnetron sputtering [19], ion beam assisted sputtering [20] and shock-wave compression of organic C-N-H precursors [11].

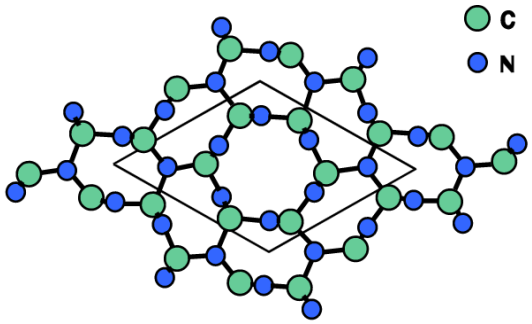

Fig. (1) The chemical structure of dicyanodiazomethane (C_3N_4) molecule

In a total reaction volume of 2000 mm^3 and gas pressure 5 mbar, the reaction of methane (CH_4) and ammonia (NH_3) needs for more than 5 ms to occur normally at room temperature and lead to the formation of cyanogen (C_2N_2) as follows [21-24]:

$$2CH_4 + 2NH_3 \rightarrow C_2N_2 + 7H_2 \qquad (1)$$

The chemical structure of cyanogen includes triple bonds between carbon and

nitrogen atoms in the form N≡C-C≡N. It is very hazardous and flammable compound [21,24].

The final product of this reaction can be varied by controlling the molar concentrations of starting materials as well as providing high power as short pulses to the reactants [5,8,17]. Then, dicyanodiazomethane (C_3N_4) can be formed as follows [25,26]:

$$3CH_4 + 4NH_3 \rightarrow C_3N_4 + 12H_2 \qquad (2)$$

The bonds between nitrogen (N) and hydrogen (H) atoms in ammonia molecule as well as those between carbon (C) and hydrogen (H) atoms in methane molecule can be easily broken by high power provided by the glow discharge [23]. Therefore, the released carbon and nitrogen atoms tend to bond with the availability of these atoms at high pressures (~3mbar).

In this work, carbon nitride (C_3N_4) nanoparticles are synthesized by a novel technique including fast glow discharge of methane and ammonia gas mixtures at high

2. Experimental Part

Deposition camber is first evacuated down to 10^{-5} mbar to remove any residuals or contaminants. Argon gas at pressure of 0.5 mbar was used to generate the fast glow discharge between two electrodes made of stainless steel. The dimensions of each electrode are 20x5 mm^2. Argon was chosen due to its low breakdown voltage (~190V at 35mA) compared to methane and ammonia, therefore, small amount (~0.033%) of the minimum applied power is consumed for the generation of plasma column to represent the resistor through which the remaining power (~99.96%) is transferred to the reaction volume to break the bonds in methane and ammonia molecules and soon induce the reaction between the released carbon and nitrogen atoms. The discharge power from a power supply (5-6kV, 4-5A) is applied between the electrodes as pulses of different durations (0.1, 0.25 and 1ms). A pulse forming network (PFN) was used to convert the DC signal of the power supply into short pulses. The repetition rate of discharge pulses could be determined from 1 to 100 Hz by the PFN circuit. However, all results presented here were obtained using repetition rate of 20 Hz. The methane (CH_4) and ammonia (NH_3) gases are premixed in a cooled reactor before pumped into the chamber at flow rate of 1 sccm. This reactor is cooled down to 5°C to prevent the normal reaction of methane and ammonia (Eq. 1). The maximum pressure of gas mixture is 3 mbar. As soon as the breakdown of argon gas occurs, the remaining power induces the reaction (Eq. 2) between CH_4 and NH_3 molecules to form C_3N_4 molecules. This reaction occurs faster than the normal reaction given by Eq. 1. The synthesized nanoparticles were collected on a clean watch glass (2cm in diameter) inside the chamber. The chamber was kept closed during the application of discharge power throughout valves on the inlets of gases and outlet to the vacuum pump. Figure (2) shows the C_3N_4 nanopowder sample prepared in this work.

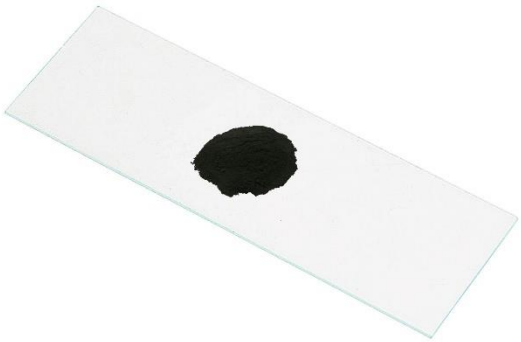

Fig. (1) Photograph of carbon nitride nanopowder prepared by in this work

3. Results and Discussion

Figure (3) shows the XRD patterns of the synthesized carbon nitride samples using fast glow discharge pulses of different durations. These patterns were illustrated with CrystalSleuth® software for XRD analysis. The sample synthesized using glow discharge pulse duration of 1 ms (Fig. 3a) shows that it is polycrystalline with twelve distinguished peaks corresponding to the crystal planes of (110), (200), (101), (210), (111), (300), (220), (310), (400), (221), (311) and (320) [1,5,18,27-30]. The number of these peaks was decreased to seven while the heights of the observed peaks were increased as the discharge pulse duration is decreased to 0.25

ms (Fig. 3b). Moreover, only three peaks are observed in the synthesized sample as the discharge pulse duration is decreased to 0.1 ms (Fig. 3c). The heights of the three observed peaks were increased. This result may be attributed to the fact that some crystal planes does not find enough time to grow at shorter pulse durations, while some other planes, such as (110), (200) and (111), are immediately formed. In other words, if the discharge power of 20-30 kW is transferred to the reaction volume during shorter time, the crystal planes produced by the reaction leading to form C_3N_4 molecules are fewer than those produced at relatively longer time. Accordingly, the crystal planes of (110), (200) and (111) seem to grow as soon as the carbon and nitrogen atoms are bonded to form C_3N_4 molecules.

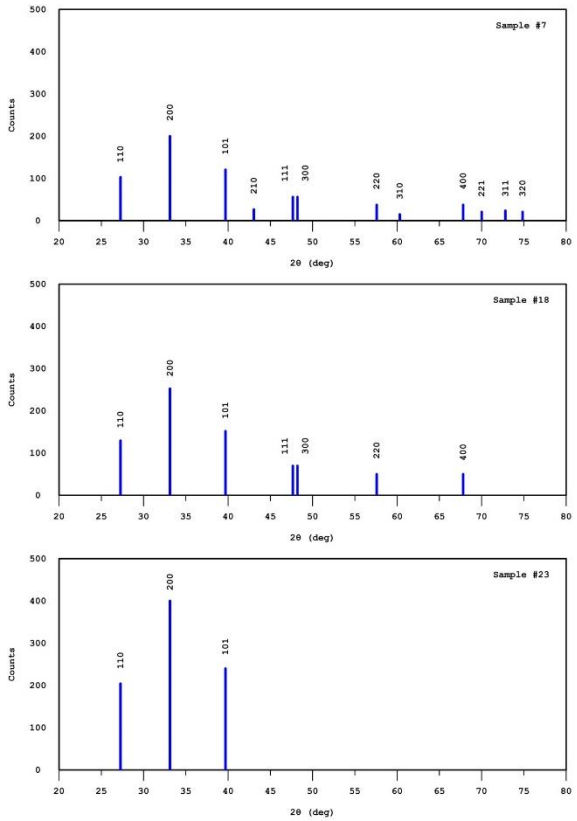

Fig. (2) The x-ray diffraction (XRD) patterns for the synthesized samples using discharge pulse duration of (upper) 1 ms, (middle) 0.25 ms, and (lower) 0.1 ms

Figure (4) shows the FTIR spectrum of the carbon nitride sample synthesized by discharge pulse duration of 0.1 ms. The broad band around 1100-1250 cm^{-1} is attributed to the stretching mode of C-N bond [5]. However, the peak at 1250 cm^{-1} is a characteristic for the sp^3-bonded C-N [8]. The peak around 1550 cm^{-1} is ascribed to the stretching mode of double C=N bond [9]. The peak around 1600 cm^{-1} is also attributed to the stretching vibration of C-N bond [13]. These peaks can be overlapped with other peaks within 1000-1800 cm^{-1} ascribed to the bonded carbon layers, which become active in the infrared region as their symmetry is broken due to the incorporation of nitrogen in these layers [30]. The peaks observed below 950 cm^{-1} are attributed to the C-H bond [8,31]. Other peaks observed around 2900 and 3340 cm^{-1} are attributed to the CH_x and NH_x groups, respectively, as precursors of carbon nitride molecules.

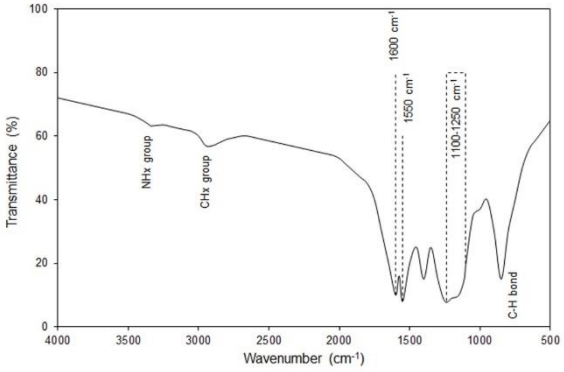

Fig. (4) The FTIR spectrum for the carbon nitride sample synthesized using discharge pulse duration of 0.1 ms

4. Conclusion

In concluding remarks, the reaction of methane (CH_4) and ammonia (NH_3) gases can be induced and controlled towards the production of carbon nitride (C_3N_4) nanoparticles without formation of cyanogen (C_2N_2). This control is performed by the application of high discharge power as short pulses to the reaction volume. The discharge pulse duration was found very important to control the number of crystal planes formed in the final product.

References

[1] X. Yuan, C. Zhou, Q. Jing, Q. Tang, Y. Mu and A. Du, *Nanomater.*, 6 (2016) 173.
[2] E.M. Fayyad, A.M. Abdullah, M.K. Hassan, A.M. Mohamed, C. Wang, G. Jarjoura and Z. Farhat, *Coatings*, 8 (2018) 37.
[3] F. Liu, Y. Ren and X. Ji, *Int. J. Mater. Sci. Eng.*, 5(4) (2017), 123-132.

[4] Dandan Zheng, Xu-Ning Cao, and Xinchen Wang, *Angew. Chem. Int. Ed.*, 55 (2016) 11512 –11516.
[5] A. Thomas, A. Fischer, F. Goettmann, M. Antonietti, J.-O. Müller, R. Schlögl and J.M. Carlsson, *J. Mater. Chem.*, 18 (2008) 4893-4908.
[6] Y. Zhao, F. Zhao, X. Wang, C. Xu, Z. Zhang, G. Shi and L. Qu, *Angew. Chem. Int. Ed.*, 53 (2014) 13934–13939.
[7] S. Elavarasan, B. Baskar, C. Senthil, Piyali Bhanja, A. Bhaumik, P. Selvam and M. Sasidharan, *RSC Adv.*, 6 (2016) 49376-49386.
[8] K.S. Khashan and M.H. Mohsin, *Surf. Rev. Lett.*, 22(4) (2015) 1550055.
[9] J. Ni and X. Hao, *Adv. Mater. Res.*, 538-541 (2012) 124-127.
[10] P.W. May, P.R. Burridge, C.A. Rego, R.S. Tsang, M.N.R. Ashfold, K.N. Rosser, R.E. Tanner, D. Cherns and R. Vincent, *Diam. Rel. Mater.*, 5 (1996) 354-358.
[11] C.M. Lieber and J. Zhang, *Adv. Mater.*, 6(6) (1994) 497-499.
[12] W.T. Zheng, X. Wang, T. Ding, X.T. Li and W.D. Fei, *Int. J. Mod. Phys. B*, 6(6-7) (2002) 1091-1095.
[13] E. Kovačević, J. Berndt, I. Stefanović, H.-W. Becker, C. Godde, Th. Strunskus, J. Winter and L. Boufendi, *J. Appl. Phys.*, 105 (2009) 104910.
[14] J.V. Badding and D.C. Nesting, *Chem. Mater.*, 8(2) (1996) 535-540.
[15] Z.Y. Fei and Y.X. Liu, *Chin. Phys. Lett.*, 20(9) (2003) 1554-1557.
[16] O.A. Hamadi, *Iraqi J. Appl. Phys. Lett. (IJAPLett)*, 1(2) (2008) 3-8.
[17] J. G. Céspedes, C. Corbella, E. Bertran, G. Viera & M. Galán, *Fullerenes, Nanotubes and Carbon Nanostructures*, 13(1) (2007) 447-455.
[18] R. Alexandrescu, F. Huisken, G. Pugna, A. Crunteanu, S. Petcu, S. Cojocaru, R. Cireasa and I. Morjan, *Appl. Phys. A*, 65 (1997) 207-213.
[19] W.T. Zheng, J.J. Li, X. Wang, X.T. Li, Z.S. Jin, B.K. Tay and C.Q. Sun, *J. Appl. Phys.*, 49(4) (2003) 2741-2745.
[20] P. Hammer, M.A. Baker, C. Lenardi and W. Gissler, *Thin Solid Films*, 290-291 (1996) 107-111.
[21] R.A. Meyers (Editor), **"Encyclopedia of Physical Science and Technology: Inorganic Chemistry"**, 3rd ed., Academic Press (2003), 828-829.
[22] P.A. Gartaganis and C.A. Winkler, *Canad. J. Chem.*, 34 (1956) 1457-1463.
[23] S.L. Miller, *Biochimica et Biophysica Acta*, 23 (1957) 480-489.
[24] P. Carson and C. Mumford, **"Hazardous Chemicals Handbook"**, Butterworth-Heinemann (Oxford, 2002), 2nd ed., 156, 233.
[25] C. Niu, Y.Z. Lu and C.M. Lieber, *Science*, 261(5119) (1993) 334-337.
[26] L.-W. Yin, M.-S. Li, Y.-X. Liu, J.-L. Sui and J.-M. Wang, *J. Phys.: Cond. Matter*, 15(2) (2003) 309-314.
[27] O. Matsumoto, T. Kotaki, H. Shikano, K. Takemura and S. Tanaka, *J. Electrochem. Soc.*, 141(2) (1994) L16-L18.
[28] Y. Gu, Y. Zhang, X. Chang, Z. Tian, N. Chen, D. Shi, X. Zhang and L. Yuan, *Sci. China Ser. A-Math.*, 43(2) (2000) 185-198.
[29] M. Arif, L.N. Blinov, R. Lappalainen and S.N. Filippov, *Glass Phys. Chem.*, 30(6) (2004) 573-575.
[30] H. Wang, "Investigations into Carbon Nitrides and Carbon Nitride Derivatives", PhD thesis, University of Munchen (Germany, 2013).
[31] V.P. Tolstoy, I.V. Chernyshova and V.A. Skryshevsky, **"Handbook of Infrared Spectroscopy of Ultrathin Films"**, Wiley-Interscience (NJ, 2003), 439
[32] O.A. Hamadi, *Proc. IMechE, Part L, Journal of Materials: Design and Applications*, 222 (2008) 65-71.
[33] A.K. Yousif and O.A. Hamadi, Bulgarian J. Phys., 35(3) (2008) 191-197.
[34] O.A. Hammadi, W.N. Raja, M.A. Saleh and W.A. Altun, *Iraqi J. Appl. Phys. (IJAP)*, 12(3) (2016) 35-42.
[35] O.A. Hammadi, *Photonic Sensors*, 6(4) (2016) 345-350.

Optimization of Magnetized Plasma Glow Discharge

Mohammed A. Hussain[1], Ali M. Ghafoori[1], Omar S. Habeeb[2]

[1] Department of Electrical Engineering, College of Engineering, University of Anbar, Ramadi, IRAQ
[2] Department of Software Engineering, College of Engineering, University of Baghdad, Baghdad, IRAQ

Abstract
In this work, a closed-field unbalanced dual magnetron assembly was designed, constructed and characterized. This assembly can be successfully used in plasma sputtering system to improve the electrical characteristics of the plasma. This improvement was shown by the Langmuir probe diagnostics of the plasma and the values of plasma parameters, such as electron and ion temperatures and densities. The applicability of such design may enhance the whole sputtering process and the production of nanoscale structures with low cost, high purity and good properties.

Keywords: Magnetron sputtering; Plasma parameters; Langmuir diagnostics; Glow discharge
Received: 02 July 2023; **Revised:** 28 July 2023; **Accepted:** 15 August 2023; **Published:** 1 October 2023

1. Introduction

Sputtering is complex process, which is highly dependent on number of process parameters, such as deposition pressure, discharge voltage, discharge current, target to substrate distance, gas compositions, process gas flow rate, reactive gas flow rate in case of reactive sputtering, substrate biasing, etc. [1-7]. Deposition of thin films by magnetron-based sputtering systems is performed at much higher rates than diodes and operated at lower pressures, where gas-phase scattering and gas-phase impurities are minimal [8-10]. DC magnetron is basically a magnetically enhanced diode in which the spatial relationship of electric and magnetic field is designed to confirm secondary electrons produced by ions bombardment of the target [11-13]. Restricting these electrons to remain close to the target surface increases their probability to ionize the working gas [14]. This effect results in more intense plasma discharge that can be sustained at lower pressure. Since the ions are heavier than electrons, they are not affected by the confining magnetic field and may sputter much as in a diode type configuration [15,16].

In case of planar circular magnetron – which is used in the present work – two round magnets are placed behind the target, as can be seen in the figure below and formation of an erosion profile known as "racetrack" is induced by the non-uniform ion bombardment across the target surface [17,18]. For balanced magnetrons, both magnets have the same magnet strength that results in strongly confined plasma near the target region [19]. Consequently, only a few charged particles reach the substrate, which might be useful in the case where low energetic bombardment is mandatory as in the case of polymeric substrates, but it is a drawback when energetic ion/electron bombardment in the anode surface is needed because the bombardment with energetic particles (ions or electrons) influence the growth of thin films [20-22].

The bombardment of the substrate with energetic particles can be achieved by unbalanced magnetron configuration, as two magnets with different strength and/or dimensions are used [23,24]. This way, the magnetic field lines are extended to the substrate and the plasma density is increased near the substrate [25-27]. Although the presence of magnets increases the efficiency of sputtering, it leads to inefficient target usage where only ~30% of the material is used [28-30].

The bulk of the plasma is "quasineutral" where electron and ion densities are the same, and the potential difference between the bulk of the plasma and the wall is concentrated in a thin layer or sheath near the wall [31]. The gradient of the plasma potential determines

the electric field that is responsible for energizing the electrons, which maintain the discharge through ionization [32].

In this work, a closed-field unbalanced dual magnetron assembly was designed, constructed and characterized to be used in plasma sputtering system to improve the electrical characteristics of the plasma. This improvement was shown by the Langmuir probe diagnostics of the plasma and the values of plasma parameters, such as electron and ion temperatures and densities.

2. Experimental Part

Two closed-field unbalanced magnetrons were employed at the anode and cathode of plasma sputtering system. Electrodes (anode and cathode) were made of stainless steel and each was a disk of 8 cm in diameter and 4 mm in thickness. Two annular concentric magnets were placed behind each electrode to form the magnetron configuration. The outer diameters of the two magnets were 8 cm and 4 cm, while the inner diameters were 4 cm and 3.2, respectively. The electrodes were connected to a DC power supply to provide the electrical power required for discharge. The lower electrode (anode) could be move vertically with respect to the fixed upper electrode (cathode) to adjust the separation of the two electrodes from 1 to 8 cm.

Pure argon gas was used to produce the discharge plasma. A DC power supply up to 5 kV was used for electrical discharge between the electrodes and both breakdown voltage (up to 1 kV) and discharge current (up to 100 mA) were monitored by two digital voltmeter and ammeter, respectively. A current limiting resistor of 6.75 kW was connected in series to the discharge circuit in order to control the current flowing in the circuit. The discharge chamber was evacuated by a two-stage Leybold-Heraeus rotary pump and the vacuum inside chamber was measured by Pirani gauge connected to a vacuum controller from Balzers VWS 120. Argon gas was supplied to the chamber through a fine-controlled needle valve (0-160 ccm) to control the gas pressure inside the chamber.

3. Results and Discussion

When dual magnetrons were used, the drained current by the probe was decreased by about 16% due to the roles of both magnetrons in trapping much more charged particles near the cathode and anode and hence reducing the number of particles passing the distance between the electrodes where the probe is placed. However, these roles could not prevent the discharge current from flowing between the electrodes but even these particles sustaining the discharge are accelerated by the both electric and magnetic fields to higher drift velocities that the probe could not attract them from their paths across the inter-electrode distance [33].

Accordingly, the magnetrons caused to change the values of plasma parameters, such as electron and ion temperatures and densities, as these parameters are deduced from the current-voltage characteristics of the probe immersed in plasma. These variations are observed in Table (1).

Table (1) Effect of using magnetrons on the plasma parameters

	No magnetron	One magnetron	Dual magnetrons
Electron Temperature (eV)	4.856	4.871	4.850
Electron Density ($x10^{21}m^{-3}$)	1.329	1.148	1.130
Ion Temperature (eV)	0.889-1.192	0.888-1.189	0.864-1.159
Ion Density ($x10^{21}m^{-3}$)	1.329	1.148	1.130

The probe current near the anode was higher by about 6% than its value at the center point because the density of electrons near the anode is already low and the magnetron at the anode also plays a role in trapping a fraction of these electrons near the anode. Therefore, the number of electrons collected by the probe near the anode is reasonably lower than that that near the cathode [34].

For comparison, the electron temperatures and densities were determined from the current-voltage characteristics of Langmuir probe for three different working pressures and at the center point between the electrodes.

As shown in Fig. (1), the electron temperature was reduced as the working pressure increased from 0.35 to 0.7mbar and then raised as the pressure increased from 0.7 to 0.9mbar.

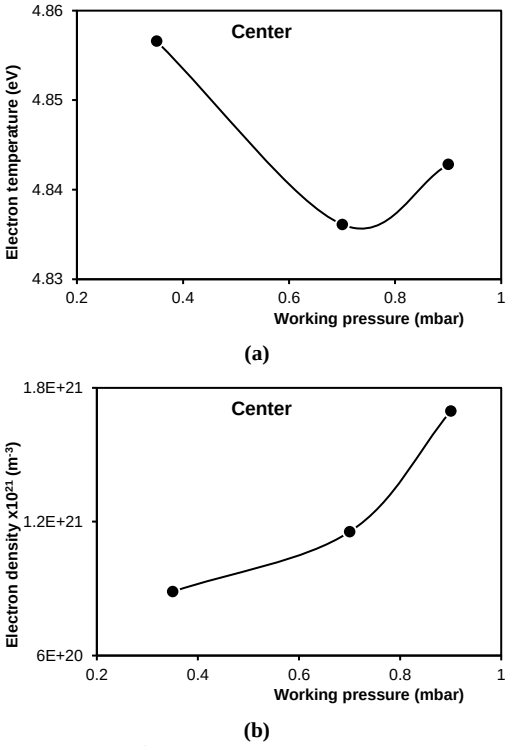

Fig. (1) Variation of electron temperature and density in plasma with working gas pressure at the center point between the electrodes when dual magnetrons were used

Increasing the working pressure means providing the discharge volume with more neutral atoms of argon and hence the mean free path of electrons as well as their gained energy is reduced as the number of their collisions with neutral atoms is decreased. Accordingly, the number of electrons produced by collisional ionization processes is decreased. The majority of these electrons are trapped by the magnetrons at both electrodes while the minority of electrons may escape from the trapping region towards the anode to sustain the glow discharge with lower energies (lower temperatures) than those trapped because they will be subject only to the electric field between the electrodes (V/d) while those trapped near the electrodes are subject to ExB drift.

A fraction of the electrons escaping from ExB trapping region may be collected by the probe at the center point between the electrodes to form the probe current, which was shown lower than those near the electrodes.

The further increase of working pressure (to 0.9mbar) provide the discharge volume with more neutral gas atoms, therefore, the number of collisions among electrons and neutral atoms is increased and hence the production of charged particles is increased too. Accordingly, the electron density is increased and more electrons are trapped by ExB effect before escaping to pass the inter-electrode distance as well as the center point where the probe is placed. These electrons are relatively higher in energy than those escaping at lower pressures (0.7mbar) because they were initially trapped before the electron density being higher than the capability of trapping region. Therefore, the probe would collect more electrons with higher energies (temperatures). Despite that ion temperatures are much lower than electron temperatures; similar behavior was observed when measured at different points between the electrodes [35].

On the other hand, the electron density (as well as ion density) was continuously increased with increasing working pressure due to the corresponding increase in discharge current, as shown earlier. The following table shows the plasma parameters deduced at three different positions between the discharge electrodes.

Table (2) Plasma parameters measured at three different positions between the discharge electrodes

	Center point	Near cathode	Near anode
Electron Temperature (eV)	4.856	4.838	4.855
Electron Density ($x10^{21}m^{-3}$)	1.130	1.654	1.201
Ion Temperature (eV)	0.864-1.159	0.885-1.188	0.869-1.166
Ion Density ($x10^{21}m^{-3}$)	1.130	1.654	1.201

4. Conclusion

The probe current was higher than other positions because the densities of electrons

near the cathode are higher than any other region inside plasma since the cathode is the source of discharge electrons in addition to the trapping effect of the magnetron placed at the cathode. Therefore, the probe would collect much more electrons in this region. The increase in probe current near the cathode was about 46% than its value at the center point between the electrodes.

The probe current near the anode was higher by about 6% than its value at the center point because the density of electrons near the anode is already low and the magnetron at the anode also plays a role in trapping a fraction of these electrons near the anode. Therefore, the number of electrons collected by the probe near the anode is reasonably lower than that that near the cathode.

References

[1] M. Lieberman, A. Lichtenberg, **Principle of plasma discharge and Material**, New York, John-Wiley and Sons (1994).

[2] G. Seriamni et al., "plasma Charactersation of a DC closed field magnetron sputtering device", ECA, 24B, 17 (2000).

[3] M. Ghoranneviss et al., "The effect of parameter of plasma of DC magnetron sputtering on properties of copper thin film deposited on glass", XXVIIth ICPIG, Eindhoven, Netherlands (2005).

[4] C. Shon et al., IEEE Transactions on plasma science", 26(6) (1998).

[5] B. Chapman, **Glow Discharge Processes**, John-Wiley & Sons, NY (1980).

[6] R. Berry, P. Hall, and M. Harris, **Thin Film Technology**, van Nostrand Reinhold Company, New York (1968).

[7] K. Hinkel, **Magnetrons**, Cleaver-Hume Press Ltd., London, 1961.

[8] J. Vossen, **Thin Film Processes**, Academic Press, Inc., New York (1978).

[9] K. Wasa and S. Hayakawa, Rev. Sci. Instrum., 40(5) (1969) 693.

[10] B. Subramanian et al., Surf. Coat. Technol., 205(21-22) (2011) 5014–5020.

[11] A. Grill, **Cold Plasma in Materials Fabrication**, IEEE, New York, 1994.

[12] N. Kumari et al., Euro. Phys. J., 59(2) (2012), Article ID 20302, 7 pages.

[13] J.A. Thornton, J. Vac. Sci. Technol., 15(2) (1978) 171–177.

[14] S.Z. Wu, J. Appl. Phys., 98 (2005), Article ID 083301, 5 pages.

[15] T.E. Sheridan, M.J. Goeckner and J. Goree, J. Vac. Sci. Technol. A, 8(30) (1990) 8 pages.

[16] S.L. Rohde et al., Thin Solid Films, 193-194(1) (1990) 117–126.

[17] R.P. Howson, H.A. J'Afer and A.G. Spencer, Thin Solid Films, 193-194(1) (1990) 127–137.

[18] S.M. Borah et al., J. Phys. D: Appl. Phys., 41(19) (2008), Article ID 195205.

[19] X.B. Zhang, J.Q. Xiao, Z.L. Pei, et al., J. Vac. Sci. Technol. A 25, 209 (2007).

[20] I. Petrov, F. Abibi, J.E. Greene, et al., J. Vac. Sci. Technol. A 10, 3283 (1992).

[21] I. Ivanov, P. Kazansky, L. Hultman, et al., J. Vac. Sci. Technol. A 12, 314 (1994).

[22] S.M. Rossnagel and H.R. Kaufman, J. Vac. Sci. Technol. A 4, 1822 (1986).

[23] T.E. Sheridan and J. Goree, J. Vac. Sci. Technol. A 7, 1014 (1989).

[24] I. Petrov, I. Ivanov, V. Orlinov, and J. Kourtev, Contrib. Plasma Phys. 30, 223 (1990).

[25] P. Spatenka, J. Vlcek, and J. Blazek, Vacuum 55, 165 (1999).

[26] L. Gu and M.A. Lieberman, J. Vac. Sci. Technol. A 6, 2960 (1988).

[27] S. Miyake, N. Shimura, T. Makabe and A. Itoh, J. Vac. Sci. Technol., A10, 1135 (1992).

[28] Q.A. Abbas, R.R. Abdula, B.T. Chiad, Iraqi J. Phys., 8(11) (2010) 41-47.

[29] B.T. Chied, R.R. Abdula, Q.A. Abbas, Iraqi J. Phys., 8(11) (2010) 33-40.

[30] S.M. Borah, J. Materials, 2013, Article ID 852859.

[31] A.A. Solov'ev et al., Plasma Physics Reports, 35(5) (2009) 399–408.

[32] E.F. Kotp and A.A. Al-Ojeery, Australian J. Basic Appl. Sci., 6(3) (2012) 817-825.

[33] B.T. Chiad, M.K. Khalaf, F.J. Kadhim, O.A. Hammadi, Characteristics and Operation Conditions of a Closed-Field Unbalanced DC Magnetron Plasma Sputtering System, J. Ind. Eng. Sci., accepted for publication, to appear in 2015

[34] M.K. Khalaf, O.A. Hammadi, F.J. Kadhim, Representation of Magnetic Field Distribution of Dual Closed-Field Unbalanced Magnetrons Employed in Glow-Discharge Plasma Sputtering System, submitted to Photonic Spectra, 2014.

[35] F.J. Kadhim, M.K. Khalaf, O.A. Hammadi, Optical and Structural Properties of Nickel Oxide Thin Films Prepared by Closed-Field Unbalanced Dual-Magnetrons Sputtering Technique, J. Optoelectron. Photon., accepted for publication, to appear in 2015.

Paschen's Curve of Argon Plasma Discharges Employed in Closed-Field Unbalanced Sputtering

Hasan M. Jasim, Raad H. Abd

Department of Physics, College of Education, Mustansiriyah University, Baghdad, IRAQ

Abstract
The effects of closed-field unbalanced dual magnetrons on the performance of plasma sputtering system were studied. These effects were introduced by comparing the obtained Paschen's curve in existence and absence of magnetrons. The distribution of magnetic fields between the magnetrons was introduced to optimize the closed-field unbalanced configuration. Characterization of Paschen's curve as well as discharge current with gas pressure at different distances between the discharge electrodes was introduced. Also, the current-voltage characteristics were introduced at the optimum operation conditions.

Keywords: Physical vapor deposition, Sputtering, Magnetron sputtering, Paschen's law
Received: 03 August 2023; **Revised:** 28 August 2023; **Accepted:** 03 September; **Published:** 1 October 2023

1. Introduction

In sputtering, at low kinetic energies (energies between 0 and about 50 eV), the ion does not have sufficient energy to dislodge the target atoms and thus the ejection of target particles occurs only for very special collision geometries [1-4]. With moderate energies (between 50 and roughly 1 keV), the ions impact dislodge "knock-on" atoms into the target, which by their turn will dislodge other target atoms [5]. Several studies showed that the ion energies must exceed four times the binding energy of the atoms of the target surface to induce sputtering. This induces collision cascade that eject atoms, ions, electrons and neutrals from the first 10 to 50Å of the surface of a target [6-9].

The breakdown voltage (V_B) depends on the product of pressure (p) and electrode separation (d) as this product is denoted as "pd", while this voltage weakly depends on the cathode material that defines the emission coefficient of secondary electrons [10-13]. As well, the breakdown voltage is proportional to the product pd at large values of this product and the electric field ($E=V/d$) is scaled linearly with the pressure [14]. In case of small values of the product pd, only few collisions occur and higher voltage is applied to increase the probability of breakdown per collision. Hence, the minimum voltage required to ignite the discharge of a gas sample of pressure p over a distance d is defined at the minimum of Paschen's curve, where

$$pd|_{V_{min}} = \frac{1}{A} log\left(1 + \frac{1}{\gamma_e}\right) \qquad (1)$$

If the pressure and/or separation distance is too large, ions generated in the gas are slowed by inelastic collisions so that they strike the cathode with insufficient energy to produce secondary electrons. In most sputtering glow discharges, the discharge starting voltage is relatively high.

Eventually, an avalanche occurs in which the ions striking the cathode release secondary electrons, which form more ions by collision with neutral gas atoms. These ions then return to the cathode, produce more electrons. When the number of electrons generated is just sufficient to produce enough electrons to regenerate the same number of electrons, the discharge is self-sustaining. The gas begins to glow, the voltage drops, and the current rises abruptly [15]. This is called the "normal glow". The color of this luminous region is characteristic of the excitation gas used. Since the secondary electron emission ratio of most materials is of the order of 0.1, more than one ion must strike a given area of the cathode to produce another secondary electron. The bombardment of the cathode in the normal

glow region self-adjusts in the area to accomplish this. Initially, the bombardment is not uniform, but concentrated near the edges of the cathode or at other irregularities on the surface. As more power is supplied, the bombardment increasingly covers the cathode surface until a nearly-uniform current density is achieved [14].

2. Experimental Part

The electrodes were connected to a DC power supply to provide the electrical power required for discharge. The lower electrode (anode) could be move vertically with respect to the fixed upper electrode (cathode) to adjust the separation of the two electrodes from 1 to 8 cm.

Pure argon gas was used to produce the discharge plasma for sputtering. A DC power supply providing voltage up to 6kV was used for electrical discharge between the electrodes and both breakdown voltage (up to 1 kV) and discharge current (up to 100 mA) were monitored by two digital voltmeter and ammeter, respectively.

First, the magnetic field intensity of each magnetron was measured individually, and second, the magnetic field intensity between both magnetrons was measured too. In the second case, the magnetrons were maintained parallel to each other and the probe was positioned between them using an adjustable clamp. Measurements were carried out over all the distance between the two magnetrons in all coordinates in order to determine the

3. Results and Discussion

In order to determine the optimum distance between two magnetrons, the magnetic field intensity was measured at the midpoint along the distance between the two magnetrons and at 2.2 cm from the edge of the electrode and the results are shown in Fig. (1). The maximum was observed at 4 cm, which can be considered as the optimum distance, while the minimum was measured at ≥ 8 cm. The diameter of the measuring probe is 0.8 cm, therefore, the minimum distance was 2 cm in order to locate the measuring probe at the midpoint. The behavior shown in the figure below is attributed to the interference between the lines of the magnetic field, i.e., the maximum interference occurs at the midpoint of 4cm separation, whereas this interference decreases as the two magnetrons move away from each other reaching to "no interference" condition at ≥ 8 cm separation.

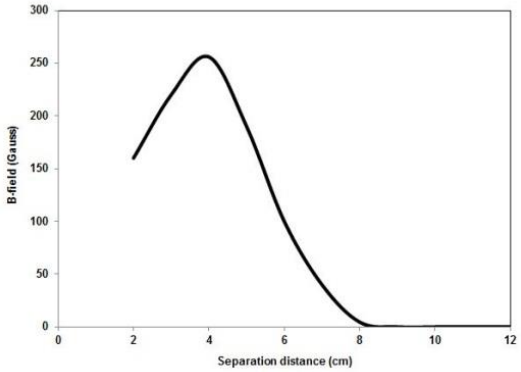

Fig. (1) Variation of magnetic field intensity along the vertical distance separating the two magnetrons

The electrons are unable to travel perpendicular to the magnetic field lines over distances greater than Larmor radius, therefore, they are confined. The electric field on the other hand causes the electrons to move in the direction perpendicular to both the electric field and the magnetic field (E×B or Hall drift) [16]. The combination of the electron confinement and the E×B drift ensures that the electrons have a much longer mean free path in the plasma than in conventional glow discharges, giving rise to more ionization collisions, and consequently higher ion fluxes [17]. These ion fluxes are highest in between the magnets, hence most of the target material is sputtered there. This gives a characteristic feature of conventional planar magnetrons called the racetrack [18]. This racetrack generally limits the complete target utilization, resulting in higher working costs [19]. This problem can be overcome by using rotatable magnetrons. Instead of a cylindrical inner magnet and an outer magnet ring, these magnetrons consist of a central bar shaped magnet surrounded by a rectangular shaped magnet configuration around which a cylindrical target rotates. This greatly enhances the utilization of the target and is

therefore much more interesting for industrial applications [20].

The sputtering electrons are assumed to be trapped near the cathode by the magnetic field of the magnetron in order to increase the path length of these electrons. Therefore, the maximum interference between the two fields is not preferred for such purpose because the electrons would not be seized near the cathode. Instead, these electrons may be drifted by the interfered lines away from the cathode.

Sputtering of a target atom is just one of the possible effects resulting from the surface ion bombardment. Aside from sputtering, the second important process is the emission of secondary electrons from the target surface, which play a fundamental role in keeping the sputtering process itself. Figure (2) shows Paschen's curve for both cases of using and not using the magnetron at the upper electrode (cathode). As clearly shown, the effect of using magnetron lies in decreasing the breakdown voltage to about 15% of its initial (maximum) value, while the minimum voltage was decreased to seventh its value in absence of magnetron. However, Paschen's curves of both cases are identical with different minima, as the value of "*p.d*" product was 1.1 mbar.cm when no magnetron is used and 1.4 mbar.cm when a magnetron is used.

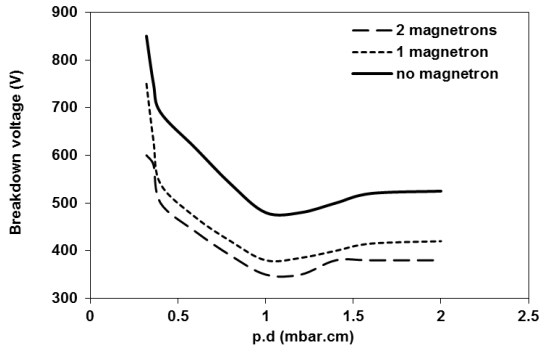

Fig. (2) Paschen's curve for the constructed plasma sputtering system with and without magnetron

A disadvantage of the magnetron sputtering configuration is that the plasma is confined near the cathode and is not available to active reactive gases in the plasma near the substrate for reactive sputter deposition. This difficulty can be overcome using an unbalanced magnetron configuration, where the magnetic field is such that some electrons can escape from the cathode region [21]. An unbalanced magnetron (UBM) has a proper magnetic field configuration in which a finite degree of the field lines from the outer magnetic pole diverge to the substrate, though the rest of the lines finish on the inner pole behind the target. Sufficient plasma density and a positive ion current on a metallic substrate even at a large distance from the target can be achieved in the unbalanced magnetron as compared with the balanced one [22,23].

The plasma sputtering system was then characterized by the relation of discharge current to the gas pressure inside the chamber at different inter-electrode distances, as shown in Fig. (3). Again, all curves are identical with the discharge current shifted upward on the vertical axis. As the distance between the electrodes is decreased, the current density from electron current emitted from the cathode $j_e(0)$ is increased because less number of electrons are able to reach the anode and hence lower current flows. However, compensation is required between gas pressure and distance to work at a given discharge current before converting into decreasing current as saturation is reached.

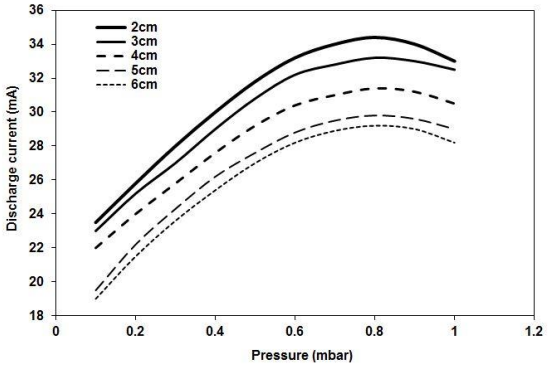

Fig. (3) Variation of discharge current with increasing gas pressure for different inter-electrode distances (*d*)

The plasma pressure will also have an impact on the sputtering process. Higher pressure means high density of gas molecules in the chamber. As a consequence, this will lead to higher electron density and ion density in the plasma. The high electron and ion

density will increase the bombardment counts and also the probability of collision between particles. The applied voltage will have an impact on the charged particles density and the energetic level of the charged particles. The density of ions is mainly related with the power input to the plasma. Usually, one thirtieth of the discharge energy will be transformed into ionization process. However, the applied voltage shouldn't reach too high for avoiding the implantation of ions.

4. Conclusion

Referring to the results obtained from this work, the home-made dc magnetron plasma sputtering system was characterized to introduce its performance in accordance to magnetic field distribution, electrical characteristics, Paschen's law and governing properties of such deposition systems. Results have showed that using magnetron at the cathode of discharge configuration highly has affected these operation characteristics as the breakdown voltage was decreased, the minimum point was little shifted upward, . This system was found to satisfy the requirements for deposition of high-quality thin films from different materials.

References

[1] E.D. McClanahan and N. Laegreid, Topics in Appl. Phys., 64 (1991) 339-377.

[2] D. Rademacher, T. Zickenrott, M. Vergöhl, Thin Solid Films 532 (2013) 98–105.

[3] J.-S. Baek and Y.J. Kim, Cooling Effect Enhancement In Magnetron Sputtering System, 5th Inter. Conf. on CFD in the Process Industries CSIRO, Melbourne, Australia 13-15 December 2006, 1-5.

[4] P.J. Kelly and R.D. Arnell, Vacuum 56 (2000) 159-172.

[5] R.D. Arnell and P.J. Kelly, Surf. Coat. Technol., 112 (1999) 170–176.

[6] J. Walkowicz et al., Tribologia, 6 (2006) 163-174.

[7] D.E. Ashenford et al., Surf. Coat. Technol., 116-119 (1999) 699-704.

[8] P. Sigmund, **Topics in Applied Physics: Sputtering by Particle Bombardment I**, ed. R. Behrisch, Vol. 47, Springer-Verlag (Berlin) 1981.

[9] F. Taherkhani and A. Taherkhani, Transaction B: Mechanical Engineering, 17(4) (2010) 253-263.

[10] G.K. Wehner and G.S. Anderson, **Vacuum Technology, Thin Films and Sputtering: An Introduction**, ed. R. V. Stuart, Academic Press, New York, 1983.

[11] A. Bogaerts et al., Spectrochimica Acta Part B 57 (2002) 609–658.

[12] E.F. Kotp and A.A. Al-Ojeery, Australian J. Basic Appl. Sci., 6(3) (2012) 817-825.

[13] S.D. Personick, Bell System Tech. J., 50(10) (1971) 3075-3095.

[14] J.-C. Wang et al., J. Appl. Phys., 113 (2013) 033301

[15] L.M. Isola, B.J. Gomez and V. Guerra, J. Phys. D: Appl. Phys., 43 (2010) 015202.

[16] T.E. Sheridan, M.J. Goeckner, and J. Goree, J. Vac. Sci. Technol. A 16(4) (1998) 2173-2176.

[17] F. Papa et al., Thin Solid Films, 520(5) (2011) 1559-1563.

[18] B. Liebig et al., Surf. Coat. Technol., 205 (2011) S312–S316.

[19] P.J. Kelly and R.D. Arnell, Surf. Coatings Technol., 112 (1999) 170-176.

[20] A.S. Penfold, in **Handbook of Thin Film Process Technology**, IOP (1995), sec. A.3.2, p. 1.

[21] B. Window and N. Savvides, J. Vac. Sci. Technol., A 4(2) (1986) 196.

[22] T. Makabe and Z. Petrovic, **Plasma Electronics: Applications in Microelectronic Device Fabrication**, Taylor & Francis, New York (2006) 301.

[23] B.T. Chiad, M.K. Khalaf, F.J. Kadhim, O.A. Hammadi, Characteristics and Operation Conditions of a Closed-Field Unbalanced DC Magnetron Plasma Sputtering System, J. Ind. Eng. Sci., accepted for publication, to appear in 2015.

Plant-Extracted Preparation of Crystalline Titanium Dioxide Nanoparticles

Zahraa H. Zaidan[1], Oday A. Hammadi[2], Kasim H. Mahmood[1]

[1] Department of Physics, College of Education for Pure Sciences, Tikrit University, Tikrit, IRAQ
[2] Department of Physics, College of Education, Al-Iraqia University, Baghdad, IRAQ

Abstract
In this work, titanium dioxide (TiO_2) nanoparticles were prepared by two different methods; solvothermal and dc reactive sputtering. The crystalline structures of these nanoparticles were determined by x-ray diffraction in order to introduce the effect of preparation method on the structural characteristics of these nanoparticles. In solvothermal method, the TiO_2 nanopowder was prepared as a nanopowder precipitated from an extract solution of banana peels and titanium isopropoxide. In dc reactive sputtering technique, the TiO_2 nanopowder was extracted from thin film samples deposited on glass substrates. Results showed that the crystalline structure of the nanopowder prepared by solvothermal method contains both anatase and rutile phases of TiO_2 with mixing ratio of 1:1, while the crystalline structure of the nanopowder prepared by dc reactive sputtering contains both anatase and rutile phases with mixing ratio of 2:1. As well, single phase (anatase) nanopowder was prepared by using heat sink method to prevent the thermal transition of anatase into rutile phase. Average crystallite size was determined for the three samples and found to be 38, 27 and 37 nm for 1:1, 2:1 and anatase samples, respectively. Accordingly, preparation method has an important role in determining the structural characteristics of the TiO_2 nanopowder and hence the preparation parameters should be sufficiently governed in order to control these characteristics.

Keywords: Titanium dioxide; Nanoparticles; Structural phase; Reactive sputtering; Solvothermal method
Received: 17 February 2023; **Revised:** 11 May 2023; **Accepted:** 18 May 2023; **Published:** 1 June 2023

1. Introduction

Crystallinity is an important factor to be considered in the optimization of the photodegradation efficiency [1,2]. It has been shown that amorphous TiO_2 has negligible photodegradation efficiency compared with TiO_2 of high crystallinity [3,4]. The low efficiency of amorphous TiO_2 is caused by the high recombination rate of electrons and holes due to the large amount of defects [5,6].

TiO_2 is close to be an ideal photocatalyst and the benchmark for photocatalysis performance [7,8]. TiO_2 is cheap, photostable in solution and nontoxic. Its holes are strongly oxidizing and redox selective [9]. For these reasons, several novel heterogeneous photocatalytic reactions have been reported at the interface of illuminated TiO_2 photocatalyst, and TiO_2-based photocatalysis has been researched exhaustively for environmental cleanup applications [10,11]. The single drawback is that it does not absorb visible light [12]. To overcome this problem, several methods including dye sensitization, doping, coupling and capping of TiO_2 are proposed [13].

In this work, titanium dioxide (TiO_2) nanoparticles were prepared by two different methods; solvothermal and dc reactive sputtering. The crystalline structures of these nanoparticles were determined by x-ray diffraction in order to introduce the effect of preparation method on the structural characteristics of these nanoparticles.

2. Experimental Part

Two methods were used in this work to prepare titanium dioxide (TiO_2) nanoparticles. In the first method, solvothermal method, the TiO_2 nanoparticles were synthesized from the titanium isopropoxide and banana peels. For more details on this work, see reference [14]. In the second method, dc reactive magnetron sputtering, a highly-pure titanium sheet was sputtered in presence of $Ar:O_2$ gas mixture inside a vacuum chamber at gas pressure of 0.5mbar and discharge current of 40mA to deposit TiO_2 thin films on glass substrates.

The deposited films were containing both rutile and anatase phases of TiO_2. In order to deposit TiO_2 films with only anatase phase, a heat sink was placed under the substrate to avoid the thermal transition of anatase into rutile phase. For more details on this technique, see references [9-13]. The nanopowder was extracted from the tin film samples by the conjunctional freezing-assisted ultrasonic extraction method [15].

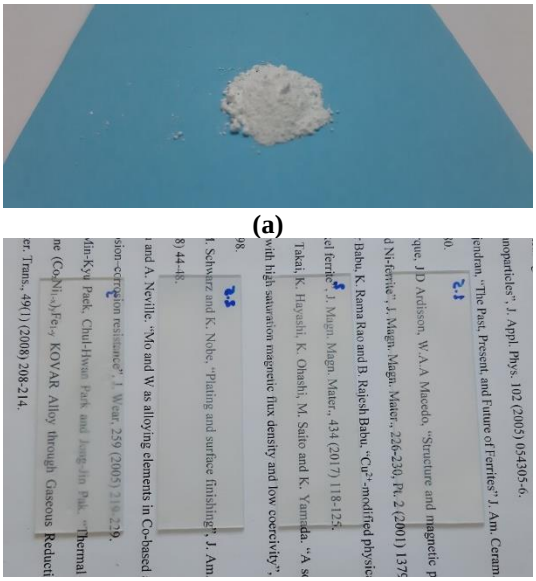

(a) **(b)**

Fig. (1) Photographs of nanopowder prepared by solvothermal method (a) and thin films prepared by dc reactive sputtering technique at different deposition times

The crystalline structures of the prepared nanopowders were determined by the x-ray diffraction (XRD) patterns obtained using a Bruker D2 PHASER XRD system (Cu-Kα x-ray tube with λ=1.54056Å).

3. Results and Discussion

Figure (2) shows the XRD patterns of the three nanopowder samples prepared in this work. It is clear that the crystalline structure of the nanopowder prepared by the solvothermal method (1:1) is identical to that of nanopowder prepared by dc reactive sputtering (2:1) without heat sink step. The difference in mixing ratio between these samples is attributed to the higher transition rate from anatase into rutile in the solvothermal method due to the inevitable thermal effect included in such preparation method, while the dc reactive sputtering technique may include limited thermal effect resulted from the heating of anode (and hence substrate) during deposition time [9]. Consequently, the transition rate from anatase into rutile is lower than that in the solvothermal method. As shown in tables (1) and (2), another difference between these two patterns is observed in the FWHM values as the 2:1 sample shows larger values of FWHM when compared to that of the 1:1 sample. This can be ascribed to the fact that sputtering is an atomic-scale preparation method while the solvothermal method is a chemical reduction method. So, the size distribution of nanoparticles formed in sputtering technique is reasonably lower than that in solvothermal method. Wider FWHM means smaller nanoparticles within the crystalline structure [16].

Table (1) XRD parameters of the 1:1 nanopowder sample

No.	Position [°2θ]	d-spacing [Å]	FWHM [°2θ]	Crystallite Size [nm]
1	25.4315	3.499	0.1624	61.5
2	27.5239	3.238	0.0758	22.6
3	36.1697	2.481	0.0866	16.0
4	37.8389	2.375	0.0758	22.8
5	41.3361	2.182	0.0866	16.2
6	48.1359	1.888	0.1948	53.3
7	53.9573	1.697	0.1948	54.7
8	54.3939	1.685	0.0792	31.3
9	55.1386	1.664	0.1848	57.5
10	62.8176	1.478	0.1584	78.1
11	69.8624	1.345	0.0792	34.0
12	75.1086	1.263	0.1320	13.2

Table (2) XRD parameters of the 4:1 nanopowder sample

No.	Position [°2θ]	d-spacing [Å]	FWHM [°2θ]	Crystallite Size [nm]
1	25.4315	3.499	0.11368	43.05
2	27.5239	3.238	0.05306	15.83
3	36.1697	2.481	0.06062	11.20
4	37.8389	2.375	0.05306	16.02
5	41.3361	2.182	0.06062	11.38
6	48.1359	1.888	0.13636	37.31
7	53.9573	1.697	0.13636	38.29
8	54.3939	1.685	0.05544	21.96
9	55.1386	1.664	0.12936	40.25
10	62.8176	1.478	0.11088	54.67
11	69.8624	1.345	0.05544	23.83
12	75.1086	1.263	0.09240	09.24

On the other hand, the nanopowder prepared by dc reactive sputtering technique with heat sink step exhibits single phase (anatase only) structure as the thermal transition was completely prevented

throughout cooling the anode (and hence the substrate) [7]. As well, the FWHM values are comparable to those of the 2:1 nanopowder sample, as shown in table (3), which is attributed to the same reason as they are both prepared by sputtering technique.

Table (3) XRD parameters of the anatase nanopowder sample

No.	Position [°2θ]	d-spacing [Å]	FWHM [°2θ]	Crystallite Size [nm]
1	25.2293	3.527	0.2814	33.5
2	38.6007	2.330	0.2598	37.7
3	47.9753	1.894	0.1948	53.2
4	55.0723	1.666	0.1732	62.8
5	62.8468	1.477	0.4330	24.5
6	68.8081	1.363	0.4330	25.4
7	75.0583	1.264	0.5196	21.9

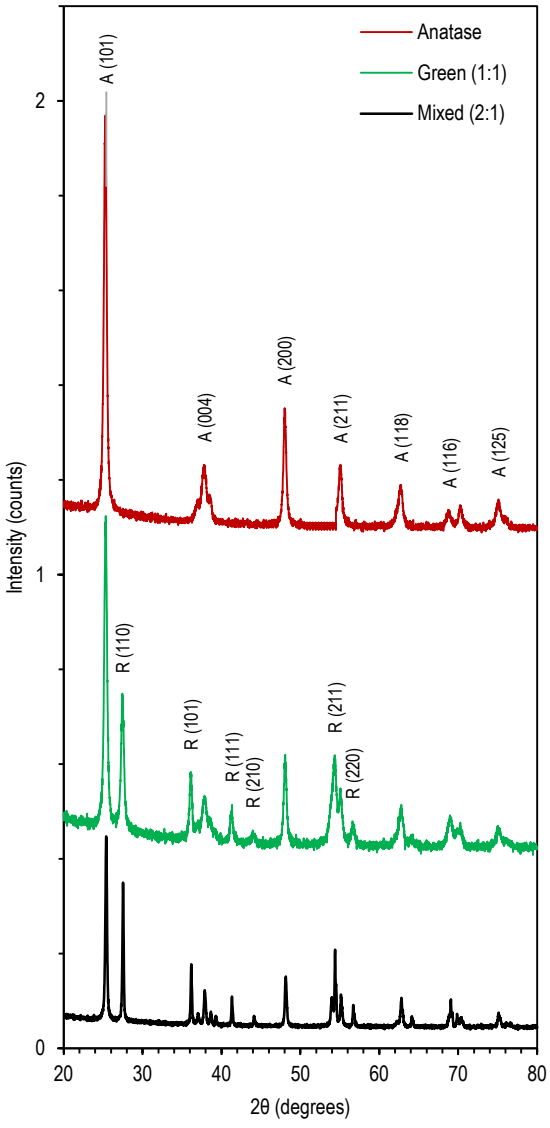

Fig. (2) XRD patterns of the three TiO_2 nanopowder samples prepared in this work

4. Conclusion

In concluding remarks, the crystalline structures of the TiO_2 nanopowders is reasonably affected by the preparation method as the preparation parameters can allow or prevent the transition of anatase phase of TiO_2 into rutile phase. Also, the average crystallite size is sufficiently affected by the preparation method as the dc reactive sputtering technique may produce mixed-phase TiO_2 nanopowder with higher anatase content and lower crystallite size. Accordingly, preparation method has an important role in determining the structural characteristics of the TiO_2 nanopowder and hence the preparation parameters should be sufficiently governed in order to control these characteristics.

References

[1] S. Rehman et al., "Strategies of making TiO_2 and ZnO visible light active", J. Hazard. Mater., 170(2-3) (2009) 560-569.

[2] A.L. Linsebigler, G. Lu, and J.T. Yates, "Photocatalysis on TiO_2 Surfaces: Principles, Mechanisms, and Selected Results", Chem. Rev., 95(3) (1995) 735-758.

[3] N.T. Nolan, "Sol-Gel Synthesis and Characterization of Novel Metal Oxide Nano-materials for Photocatalytic Applications", Ph.D. thesis, Dublin Institute of Technology, Ireland (2010).

[4] K. Eufinger, "Effect of deposition conditions and doping on the structure, optical properties and photocatalytic activity of d.c. magnetron sputtered TiO_2 thin films", Ph.D. thesis, Ghent University, Belgium (2007).

[5] O. Carp, C.L. Huisman and A. Reller, "Photoinduced reactivity of titanium dioxide", Prog. Sol. Stat. Chem., 32 (2004) 33-117.

[6] O.A. Hammadi, F.J. Kadhim and E.A. Al-Oubidy, "Photocatalytic Activity of Nitrogen-Doped Titanium Dioxide Nanostructures Synthesized by DC Reactive Magnetron Sputtering Technique", Nonl. Opt. Quantum Opt., 51(1-2) (2019) 67-78.

[7] E.A. Al-Oubidy and F.J. Al-Maliki, "Photocatalytic activity of anatase titanium dioxide nanostructures prepared by reactive magnetron sputtering technique", Opt. Quantum Electron., 51(1-2) (2019) 23.

[8] E.A. Al-Oubidy and F.J. Al-Maliki, "Effect of Gas Mixing Ratio on Energy Band Gap of Mixed-Phase Titanium Dioxide Nanostructures Prepared by Reactive Magnetron Sputtering Technique", Iraqi J. Appl. Phys., 14(4) (2018) 19-23.

[9] F.J. Al-Maliki, O.A. Hammadi and E.A. Al-Oubidy, "Optimization of Rutile/Anatase Ratio in Titanium Dioxide Nanostructures prepared by DC Magnetron Sputtering Technique", Iraqi J. Sci., 60(special issue) (2019) 91-98.

[10] F.J. Al-Maliki and E.A. Al-Oubidy, "Effect of gas mixing ratio on structural characteristics of titanium dioxide nanostructures synthesized by DC reactive magnetron sputtering", Physica B: Cond. Matter, 555 (2019) 18-20
[11] F.J. Al-Maliki, O.A. Hammadi, B.T. Chiad and E.A. Al-Oubidy, "Enhanced photocatalytic activity of Ag-doped TiO_2 nanoparticles synthesized by DC Reactive Magnetron Co-Sputtering Technique", Opt. Quantum Electron., 52 (2020) 188.
[12] R.A.H. Hassan and F.T. Ibrahim, "Preparation and Characterization of Anatase Titanium Dioxide Nanostructures as Smart and Self-Cleaned Surfaces", Iraqi J. Appl. Phys., 16(4) (2020) 13-18.
[13] M.A. Hameed, S.H. Faisal, R.H. Turki, "Characterization of Multilayer Highly-Pure Metal Oxide Structures Prepared by DC Reactive Magnetron Sputtering Technique", Iraqi J. Appl. Phys., 16(4) (2020) 25-30
[14] Z.H. Zaidan, K.H. Mahmood and O.A. Hammadi, "Using Banana Peels for Green Synthesis of Mixed-Phase Titanium Dioxide Nanopowders", Iraqi J. Appl. Phys., 18(4) (2022) 27-30.
[15] O.A. Hammadi, "Production of Nanopowders from Physical Vapor Deposited Films on Nonmetallic Substrates by Conjunctional Freezing-Assisted Ultrasonic Extraction Method", Proc. IMechE, Part N, J. Nanomater. Nanoeng. Nanosys., 232(4) (2018) 135-140.
[16] A. Zachariah et al., "Synergistic Effect in Photocatalysis As Observed for Mixed-Phase Nanocrystalline Titania Processed via Sol-Gel Solvent Mixing and Calcination", J. Phys. Chem. C, 112 (2008) 11345-11356.

IRAQI JOURNAL OF APPLIED PHYSICS LETTERS
EDITORIAL BOARD

COPYRIGHT RELEASE FORM

IRAQI JOURNAL OF
APPLIED PHYSICS LETTERS (IJAPLett)

We, the undersigned, the author/authors of the article titled

……
……
……
……
……
……
……

that is submitted to the Iraqi Journal of Applied Physics Letters (IJAPLett) for publication, declare that we have neither taken part or full text from any published work by others, nor presented or published it elsewhere in any other journal. We also declare transferring copyrights and conduct of this article to the Iraqi Journal of Applied Physics Letters (IJAPLett) after accepting it for publication.

The authors will keep the following rights:

1. Possession of the article such as patent rights.
2. Free of charge use of the article or part of it in any future work by the authors such as books and lecture notes after informing IJAP editorial board.
3. Republishing the article for any personal purposes of the authors after taking journal permission.

To be signed by all authors:

Signature:……..date: ……
Printed name: ……

Signature:……..date: ……
Printed name: ……

Signature:……..date: ……
Printed name: ……

Correspondence author:……...
……
Address:……
……
Telephone:……..……..email: ……

Note: Complete and sign this form and mail it to the below address with your finally revised manuscript

The Iraqi Journal of Applied Physics Letters
P. O. Box 88052, Baghdad 12631, IRAQ
www.iraqiphysicsjournal.com
Email: editor@iraqiphysicsjournal.com
Email: editor_ijap@yahoo.co.uk
Email: ijaplett.editor@gmail.com

IRAQI JOURNAL OF APPLIED PHYSICS LETTERS
Volume (6) Issue (4) October-December 2023

CONTENTS